Contents lists available at ScienceDirect

Phytochemistry

Phytotoxic *neo*-clerodane diterpenoids from the aerial parts of *Scutellaria barbata*

Hang-Ying Li, Wen-Jun Wei, Kai-Liang Ma, Jie-Yao Zhang, Ya Li[**], Kun Gao[*]

State Key Laboratory of Applied Organic Chemistry, College of Chemistry and Chemical Engineering, Lanzhou University, Lanzhou, 730000, China

ARTICLE INFO

ABSTRACT

Bioactivity guided the isolation of extracts from the aerial parts *Scutellaria barbata* D. Don to discover *neo*-clerodane diterpenoids with potent phytotoxic activity. Of the 34 isolates, 13 *neo*-clerodane diterpenoids were described for the first time. The structures of these undescribed compounds were elucidated by extensive analysis of NMR spectroscopic data, and the absolute configurations of scutebarbolides A and L and scutebata W were determined by X-ray diffraction. The phytotoxic activity of all compounds against the growth of the roots and shoots of *L. perenne* and *L. sativa* seedlings were first reported, and some compounds showed considerable inhibitory effects, especially scutebarbolide K, whose inhibition rates were higher than those of the positive control at concentrations ranging from 25 to 200 μg/mL. When L. *perenne* and *L. sativa* seedlings were treated at a concentration of 200 μg/mL, scutebarbolide K caused wilting symptoms on and finally death of these two tested plant seedlings. In addition, the structure-activity relationships of these *neo*-clerodane diterpenoids were also discussed.

1. Introduction

Weeds are one of the important biological factors endangering crop growth and reducing yield by competing with crops for water, nutrients and light (Shaik et al., 2017; Tshewang et al., 2016). At present, weeds can be controlled by a variety of means including manual, mechanical, physical, and chemical weedings (Zhao et al., 2017). Chemical weeding is still the most common choice because it is highly efficient, timeless, labor-saving, and economical. Synthetic herbicides can be of some help for farmers and gardeners – but they also come with drawbacks, such as harm to environment, wildlife, and humans (Macías et al., 2000; Tucci et al., 2019; Owen and Zelaya, 2005). This prompted us to look for herbicides from natural sources due to their advantages of being renewable, environmentally friendly, and less harmful to wildlife and humans.

Scutellaria barbata D. Don is a perennial herb plant of the genus *Scutellaria* in the Lamiaceae, distributed widely in China, Korea, India, and other Asian countries, and is popularly used in China as a traditional medicine for the treatment of various diseases (Yeon et al., 2015; Yang et al., 2017). The chemical constituents of this plant have been widely studied, having led to the isolation of *neo*-clerodane diterpenoids, diterpenoid alkaloids, and flavonoids (Dai et al., 2011; Zhu et al., 2011; Li et al., 2014a, 2014b; Wu et al., 2015; Wang et al., 2012, 2018,

2019; Guo et al., 2019). Some *neo*-clerodane diterpenoids have been reported to possess brilliant phytotoxic activity (Bisio et al., 2011; Li et al., 2014a, 2014b). A bioassay-guided isolation approach to *S. barbata* was performed, which revealed that the EtOAc fraction showed a better phytotoxic activity than the *n*-BuOH fraction. Thus, a phytochemical investigation of the EtOAc fraction led to 34 *neo*-clerodane diterpenoids (13 previously undescribed ones). The phytotoxic activity of these purified compounds was also evaluated. Herein, the isolation, structural characterization, and phytotoxic activity of these *neo*-clerodane diterpenoids are described. To the best of our knowledge, this is the first report on the phytotoxic activity of *neo*-clerodane diterpenoids from *S. barbata*.

2. Results and discussion

2.1. Structure identification of those undescribed compounds

Compounds **1–4**, **5–7**, **8–23** (except **9**, **10**, **17**, and **19**) display the same features but different 6,7 substitution. The existence in **1 − 23** of one ester carbonyl carbon, and two (or three) double bonds (three or four IOHDs) were evidenced by the ^{1}H NMR and ^{13}C NMR signals (Tables 1 − 4), as well as the presence of different substituents, with the remaining carbon resonances pointing out the tricyclic (**2**, **10**, and **11**
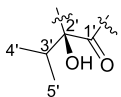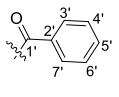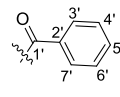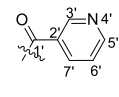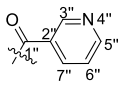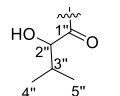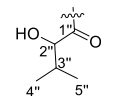
Table 1

^{1}H NMR spectroscopic data of compounds **1**, **2**, and **5–9** (δ in ppm, in CDCl$_3$, J in Hz).

position	1[a]	2[c]	5[a]	6[a]	7[a]	8[a]	9[c]
1a	1.92, dd (11.4, 7.2)	1.91, m	1.94, d (11.4)	1.84, m	1.79, m	1.74, m	1.64, m
1b	1.72, m	1.75, m	1.72, m	1.82, m	1.61, m	1.13, m	1.53, m
2a	2.08, m	2.10, m	2.09, m	2.16, m	2.11, m	2.12, m	2.04, m
2b	1.84, m	1.86, m	1.81, m	1.54, m	2.06, m	1.48, m	1.84, m
3	5.26, br s	5.25, br s	5.25, br s	5.29, br s	5.27, br s	5.26, br s	5.23, br s
6	5.01, d (9.6)	4.15, d (9.6)	3.64, d (9.6)	5.82, d (10.2)	5.59, d (10.8)	5.64, d (10.2)	3.28, d (7.2)
7	3.71, dd (9.6, 6.0)	4.45, d (9.6)	3.61, d (9.6)	5.71, d (10.2)	5.51, d (10.8)	5.49, d (10.2)	3.43, d (7.2)
8							1.56, m
10	2.19, d (11.4)	2.21, m	2.18, d (11.4)	2.53, d (12.0)	2.43, d (12.0)	2.29, m	1.41, m
11a	5.61, d (10.8)	5.59, d (10.5)	5.53, d (10.2)	5.59, d (10.2)	5.53, d (10.8)	1.94, m	1.66, m
11b						1.62, m	1.58, m
12a	3.52, d (15.0)	3.45, d (15.3)	3.37, d (14.4)	3.44, d (14.4)	3.31, d (15.0)	3.09, m	2.22, m
12b	2.60, dd (15.0, 10.8)	2.63, m	2.49, dd (10.2, 14.4)	2.69, dd (10.2, 14.4)	2.71, dd (10.8, 15.0)	2.31, m	1.22, m
14a	5.84, s	5.84, s				5.83, m	5.85, s
16a	4.89, d (17.4)	4.89, d (17.7)	4.74, d (16.2)	4.74, d (13.8)	4.79, d (16.2)	4.74, br s	4.74, d (1.5)
16b	4.67, d (17.4)	4.67, d (17.7)	4.56, d (16.2)	4.53, d (13.8)	4.58, d (16.2)		
17	1.36, s	1.44, s	1.37, s	1.33, s	1.26, s	1.16, s	1.00, d (6.6)
18	1.59, s	1.80, s	1.83, s	1.58, s	1.54, s	1.52, s	1.84, s
19	1.18, s	1.15, s	1.09, s	1.46, s	1.41, s	1.40, s	1.08, s
20	0.82, s	0.85, s	0.81, s	1.01, s	0.95, s	1.01, s	0.83, s
	-OCOCH$_3$						

		2[c]		6[a]	7[a]	8[a]	

position	1[a]	2[c]	5[a]	6[a]	7[a]	8[a]	9[c]
2′	2.12, s						
3′		2.21, m		7.75, br d (7.8)	8.01, br d (7.8)	9.18, s	
4′		1.05, d (6.9)		7.42, t (7.8)	7.46, t (7.8)		
5′		0.96, d (6.9)		7.24, br t (7.8)	7.58, br t (7.8)	8.77, d (4.8)	
6′				7.42, t (7.8)	7.46, t (7.8)	7.41, dd (4.8, 7.8)	
7′				7.75, bt d (7.8)	8.01, br d (7.8)	8.26, d (7.8)	
2″					3.73, d (7.2)	3.75, d (3.6)	
3″				9.05, s	1.93, m	1.91, m	
4″					0.84, d (7.2)	0.87, d (7.2)	
5″				8.68, d (4.2)	0.71, d (7.2)	0.74, d (7.2)	
6″				7.22, t (4.2)			
7″				8.05, d (4.2)			
11	-OCOCH$_3$	-OCOCH$_3$	-OCOCH$_3$	-OCOCH$_3$	-OCOCH$_3$		
2‴	2.03, s	2.04, s	2.05, s	2.07, s	2.05, s		

[b] Data were recorded at 400 MHz.

[a] Data were recorded at 600 MHz.

[c] Data were recorded at 300 MHz.

one extra cycle) *neo*-cleroda-di(tri)en-15,16-olide structure, quite common amongst the isolates from *S. barbata* [about 60 previously reported compounds possessed *neo*-cleroda-di(tri)en-15,16-olide skeleton (Wang et al., 2019)]. Scutebarbolides A−J possess a butenolide side chain, and scutebarbolides K−M displayed a 13-spiro-15,16-lactone skeleton, all with the same relative configurations at C-5, C-6, C-7, C-8, C-9, and C-10 as those reported for scutebarbolide A, based on the same NOESY correlations H-6/H-10 and H-7/H$_3$-17, H$_3$-19, and H$_3$-20, whereas correlations H-11/H$_3$-17 and H$_3$-20 pointed out the relative C-11 configuration of scutebarbolides A−E as (*S**).

Scutebarbolide A (**1**), in the form of colorless needles, exhibited a molecular formula of C$_{24}$H$_{34}$O$_8$ based on the analysis of the HRESIMS data (*m/z* 451.2333 [M + H]$^+$, calcd, 451.2326) and 1D NMR data (Tables 1 and 3), which required eight indices of hydrogen deficiency (IOHDs). Its IR spectrum showed absorption bands for hydroxy (3456 cm^{-1}), α,β-unsaturated lactone (1739 cm^{-1}), and olefinic (1640 cm^{-1}) functionalities. The existence of two typical acetyl groups (two IOHDs fullfiled), was evidenced by the ^{1}H NMR [δ_H 2.12 (s, H$_3$-2′) and 2.03 (s, H$_3$-2‴)] and ^{13}C NMR signals [δ_C 174.1 (C-1′) and 20.9 (C-2′); 170.9 (C-1‴) and 20.8 (C-2‴)]. Besides, the remaining 20 carbon resonances were attributed to one ester carbonyl carbon, four quaternary carbons (two olefinic ones), one oxygenated tertiary carbon, six

methines (three oxygenated and two olefinic ones), four methylenes (one oxygenated carbon), and four methyls according to the ^{13}C NMR and HSQC spectra. A tricyclic structure was required for **1** to fulfill the remaining three indices.

Analysis of the ^{1}H–^{1}H COSY confirmed three structural fragments appropriated for a *neo*-clerodane structure: **a** CH(10)−CH$_2$(1)−CH$_2$(2)−CH(3), **b** CH(6)−CH(7), and **c** CH(11)−CH$_2$(12), which were drawn with red bold bonds in Fig. 2a. The HMBC correlations from H-3 to C-5, from H-6 to C-4, C-5, and C-10, from H-7 to C-8, from H-10 to C-4, C-5, C-8, and C-9, from H$_3$-17 to C-7, C-8, and C-9, from H$_3$-18 to C-3, C-4, and C-5, from H$_3$-19 to C-4, C-5, and C-6, and from H$_3$-20 to C-8, C-9, and C-10 connected fragment **a** with fragment **b**, and simultaneously constructed the A- and B-rings. The ring C was achieved by the HMBC cross-peaks from H-14 to C-13, C-15, and C-16 and from H$_2$-16 to C-13, C-14, and C-15. And the HMBC cross-peaks from H-11 to C-9 and H$_2$-12 to C-13 revealed that fragment **c** joined the C-ring and B-ring. Moreover, the attachment of the two acetyl groups at C-6 and C-11 was confirmed by the key HMBC correlations of H-6 (δ_H 5.01, d, J = 9.6 Hz) with C-1′ (δ_C 174.1) and of H-11 (δ_H 5.61, d, J = 10.8 Hz) with C-1″ (δ_C 170.9). Considering the chemical shifts of C-7 (δ_C 74.9) and C-8 (δ_C 78.8) and the HMBC correlations from H-7 and H$_3$-17 to C-8, two hydroxy groups were located at C-

Table 2

^{1}H NMR spectroscopic data of compounds **10**, **11**, **14**, **25**, **27**, and **30** (δ in ppm, in CDCl$_3$, J in Hz).

position	10[a]	11[b]	14[b]	25[a]	27[a]	30[b]
1a	1.64, m	1.59, m	1.58, m	5.13, dd (13.2, 6.0)	5.38, m	2.37, m
1b	1.58, m	1.31, m	1.27, m			2.34, m
2a	2.12, m	2.14, m	2.00, m	2.71, d (13.2)	2.61, m	2.05, m
2b	2.00, m	1.88, m	1.97, m	2.12, m	2.03, m	2.04, m
3	5.24, br s	5.27, s	5.18, br s	5.31, br s	5.29, s	5.39, br s
6	3.78, d (9.0)	4.28, d (9.6)	4.08, dd (4.8, 9.6)	3.66, d (9.0)	5.37, d (11.4)	5.24, d (10.0)
7	4.30, t (9.0)	4.51, d (9.6)	5.25, d (9.6)	3.44, d (9.0)	5.23, d (11.4)	5.20, d (10.0)
8	1.71, m					
10	1.50, m	2.09, m	2.12, m	2.50, d (6.0)	2.51, m	2.37, m
11a	1.73, m	6.32, d (16.8)	6.35, d (16.8)	1.99, m	1.94, m	5.38, br s
11b	1.62, m			1.52, m	1.61, m	
12a	2.24, m	6.45, d (16.8)	6.41, d (16.8)	2.13, m	1.96, m	2.01, m
12b	1.18, m			1.31, m	1.71, m	2.01, m
14a	5.86, s	5.93, s	5.89, s	2.79, d (17.4)	3.11, d (17.4)	3.13, d (17.6)
14b				2.55, d (17.4)	2.54, d (17.4)	2.61, d (17.6)
16a	4.75, d (1.2)	5.21, d (16.5)	5.02, d (16.4)	4.22, d (9.0)	4.22, d (9.0)	4.37, d (8.8)
16b	4.75, d (1.2)	5.05, d (16.5)	4.97, d (16.4)	4.17, d (9.0)	4.13, d (9.0)	4.19, d (8.8)
17	1.05, d (1.2)	1.21, s	1.03, s	1.41, s	1.29, s	1.29, s
18	1.82, s	1.81, s	1.84, s	1.94, s	1.64, s	1.58, s
19	1.15, s	1.17, s	1.21, s	1.18, s	1.28, s	1.20, s
20	0.88, s	1.12, s	1.13, s	1.05, s	1.05, s	1.05, s
					-OCOCH$_3$	-OCOCH$_3$
2′					2.01, s	2.08, s
3′	2.22, m	2.27, t (6.6)	2.03, m	7.97, br d (7.8)		
4′	1.07, d (6.6)	1.08, d (6.6)	0.99, d (4.4)	7.47, t (7.8)		
5′	0.99, d (6.6)	0.99, d (6.6)	0.96, d (4.4)	7.60, br t (7.8)		
6′a			3.02, d (16.8)	7.47, t (7.8)		
6′b			2.78, d (16.8)			
7′				7.97, br d (7.8)		
8′			3.69, s			
					-OCOCH$_3$	-OCOCH$_3$
2″					1.99, s	1.99, s
					-OCOCH$_3$	-OCOCH$_3$
2‴					2.07, s	2.10, s

^{c}Data were recorded at 300 MHz.

^{a} Data were recorded at 600 MHz.

^{b} Data were recorded at 400 MHz.

7 and C-8, respectively (see Fig. 3).

The relative configuration of **1** was verified by the NOESY signals (Fig. 2b). The NOESY correlations between H-6/H-10 and H-7/H$_3$-17, H$_3$-19, and H$_3$-20 revealed that H-6 and H-10 were β-oriented and H-7, Me-17, Me-19, and Me-20 were α-oriented. In addition, a (11S^*)-configuration was deduced from the NOESY correlations of H-11/H$_3$-17 and H$_3$-20 (Zhu et al., 2010). The single-crystal X-ray diffraction experiment (Cu Kα radiation) further corroborated the planar structure and fully determined its absolute configuration as (5R,6R,7S,8R,9S,10S,11S) with a Flack parameter of 0.00(9) (Flack and Bernardinelli, 1999). Scutebarbolide A was also defined as (5R,6R,7S,8R,9S,10S,11S)-6,11-diacetoxy-7,8-dihydroxy-*neo*-cleroda-3,13-dien-15,16-olide. The same pattern but different C-6/C-7 substitution is present in scutebarbolide B (**2**) [6α(2′),7β(1′)-(2β-hydroxy-3-methylbutyryl)dioxy], the two known scutebata W (**3**) [6α-(2-hydroxy-2-methoxycarbonylmethyl-3-methyl)butyryloxy] (Yang et al., 2017), and scutolide J (**4**) (6α,7β-dinicotinoyloxy) also isolated in the present work, as well as in scutolides F (6α-benzoyloxy), G (7β-isobutyryloxy), H (6α-nicotinoyloxy-7β-isobutyryloxy), I (7β-acetoxy) (Wu et al., 2015).
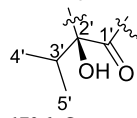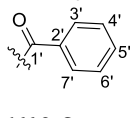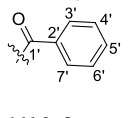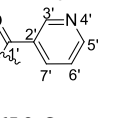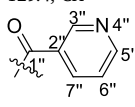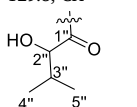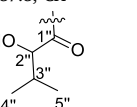
Scutebarbolide B (**2**) had a molecular formula of C$_{27}$H$_{38}$O$_9$ as determined by the HRESIMS data (*m/z* 529.2408 [M + Na]$^+$, calcd, 529.2408) and ^{13}C NMR spectrum, implying nine IOHDs. The different C-6/C-7 substitution [6α(2′),7β(1′)-(2β-hydroxy-3-methylbutyryl)dioxy] is present in scutebarbolide B (**2**), which was established from its

^{1}H and ^{13}C NMR spectra [δ_H 2.21 (m, H-3′), 1.05 (d, J = 6.9 Hz, H$_3$-4′), and 0.96 (d, J = 6.9 Hz, H$_3$-5′); δc 170.6 (C-1′), 99.1 (C-2′), 36.7 (C-3′), 17.3 (C-5′), and 14.4 (C-4′)], the ^{1}H–^{1}H COSY correlations of H$_3$-4′/H-3′/H$_3$-5′, the key HMBC cross-peaks from H-3′ to C-1′, C-2′, C-4′, and C-5′, from H$_3$-4′ to C-2′ and C-3′, and from H$_3$-5′ to C-2′ and C-3′, the ^{13}C NMR chemical shift at C-7 (δc 84.2), and the key HMBC correlation of H-6 (δ_H 4.15, d, J = 9.9 Hz) with C-2′. Thus, the 2D structure was elucidated as depicted in Fig. 1. The NOESY correlations of H-7 with H$_3$-4′ and H$_3$-5′ suggested that OH-2′ was β-oriented. Scutebarbolide B was named as (11S^*)-11-acetoxy-8β-hydroxy-6α(2′),7β(1′)-(2β-hydroxy-3-methylbutyroyl)dioxy-*neo*- cleroda-3,13-dien-15,16-olide.

Scutebarbolide C (**5**) had the molecular formula C$_{22}$H$_{32}$O$_8$ according to the HRESIMS data (*m/z* 425.2176 [M + H]$^+$ calcd for C$_{22}$H$_{33}$O$_8$ 425.2170) and ^{13}C NMR spectrum. Scutebarbolide C was the 6,14-dihydroxy analogue of **1**, which was confirmed by the ^{1}H–^{1}H COSY correlation of H-6/H-7, the HMBC correlations from H-6 to C-5, C-8, and C-10, and from H$_2$-16 to C-13, C-14, and C-15. The ^{1}H–^{1}H COSY, HSQC, HMBC, and NOESY data further confirmed that the structure of **5** was (11S^*)-11-acetoxy-6α,7β,8β,14-tetrahydroxy-*neo*-cleroda-3,13-dien-15,16-olide.

Scutebarbolide D (**6**) showed a [M + H]$^+$ ion at *m/z* 634.2664 (calcd 634.2647) in the HRESIMS spectrum, consistent with a molecular formula of C$_{35}$H$_{39}$NO$_{10}$. The NMR data (Tables 1 and 3) pointed out the presence of signals for a benzoyloxy group [δ_H 7.75 (d, J = 7.8 Hz, H-3′ and H-7′), 7.42 (t, J = 7.8 Hz, H-4′ and H-6′), and 7.24

Table 3
^{13}C NMR spectroscopic data of compounds 1, 2, and 5–9 (δ in ppm, in CDCl$_3$).

position	1[a]	2[c]	5[a]	6[a]	7[a]	8[a]	9[c]
1	19.5, CH$_2$	19.3, CH$_2$	19.7, CH$_2$	19.6, CH$_2$	19.5, CH$_2$	18.6, CH$_2$	17.9, CH$_2$
2	26.0, CH$_2$	25.9, CH$_2$	26.1, CH$_2$	25.9, CH$_2$	25.9, CH$_2$	26.2, CH$_2$	26.2, CH$_2$
3	123.4, CH	122.2, CH	122.5, CH	123.3, C	123.5, C	123.5, C	122.2, CH
4	141.5, C	142.7, C	143.2, C	141.4, C	141.3, C	141.1, C	143.4, C
5	42.5, C	42.2, C	43.1, C	43.2, C	43.2, C	43.5, C	43.6, C
6	77.1, CH	71.8, CH	75.8, C	75.4, CH	75.0, CH	76.4, CH	80.5, CH
7	74.9, CH	84.2, CH	75.2, C	77.4, CH	75.4, CH	77.3, CH	74.6, CH
8	78.8, C	77.3, C	78.4, C	78.5, C	78.5, C	70.1, C	40.9, CH
9	46.9, C	47.2, C	47.0, C	47.6, C	47.4, C	42.7, C	39.2, C
10	40.4, CH	40.4, CH	40.3, CH	40.6, CH	40.5, CH	40.4, CH	45.1, CH
11	74.9, CH	74.4, CH	76.3, CH	75.6, CH	77.2, CH	35.3, CH$_2$	35.6, CH$_2$
12	33.0, CH$_2$	32.9, CH$_2$	28.7, CH$_2$	28.9, CH$_2$	28.8, CH$_2$	25.0, CH$_2$	22.4, CH$_2$
13	168.4, C	168.2, C	131.1, C	129.9, C	129.0, C	171.8, C	170.5, C
14	116.8, CH	116.7, CH	138.4, C	138.6, C	138.2, C	114.5, C	115.3, CH
15	173.9, C	174.2, C	171.2, C	171.1, C	170.6, C	174.0, C	174.1, C
16	73.3, CH$_2$	73.3, CH$_2$	70.0, CH$_2$	69.8, CH$_2$	69.8, CH$_2$	73.4, CH$_2$	73.2, CH$_2$
17	22.0, CH$_3$	21.1, CH$_3$	22.1, CH$_3$	22.2, CH$_3$	22.4, CH$_3$	21.9, CH$_3$	11.2, CH$_3$
18	20.8, CH$_3$	22.1, CH$_3$	22.5, CH$_3$	20.5, CH$_3$	20.5, CH$_3$	20.4, CH$_3$	22.1, CH$_3$
19	17.4, CH$_3$	16.5, CH$_3$	16.1, CH$_3$	17.4, CH$_3$	17.4, CH$_3$	17.5, CH$_3$	16.5, CH$_3$
20	16.3, CH$_3$	16.3, CH$_3$	16.4, CH$_3$	16.4, CH$_3$	16.3, CH$_3$	21.7, CH$_3$	19.1, CH$_3$
6	-OCOCH$_3$	[2-hydroxy-methylbutyryl fragment: 2′ 1′, 4′ 3′, OH O, 5′]		[benzoyl: O, 1′ 2′ 3′ 4′ 5′ 6′ 7′]	[benzoyl: O, 1′ 2′ 3′ 4′ 5′ 6′ 7′]	[nicotinoyl: O, 1′ 2′ 3′ N4′ 5′ 6′ 7′]	
1′	174.1, C	170.6, C		166.2, C	166.3, C	165.2, C	
2′	20.9, CH$_3$	99.1, C		130.0, C	129.6, C	126.0, C	
3′		36.7, CH		129.4, CH	129.8, CH	151.0, CH	
4′		14.4, CH$_3$		128.4, CH	128.7, CH		
5′		17.3, CH$_3$		133.2, C	133.6, C	153.9, CH	
6′				128.4, CH	128.7, CH	123.7, CH	
7′				129.4, CH	129.8, CH	137.3, CH	
7				[nicotinoyl: O, 1″ 2″ 3″ N4″ 5″ 6″ 7″]	[HO, 1″ 2″ 3″ 4″ 5″]	[HO, 1″ 2″ 3″ 4″ 5″]	
1″				164.5, C	173.8, C	174.4, C	
2″				125.4, C	75.3, CH	75.4, CH	
3″				150.5, CH	29.3, CH	31.8, CH	
4″					19.2, CH$_3$	19.3, CH$_3$	
5″				152.8, CH	15.8, CH$_3$	15.9, CH$_3$	
6″				123.5, CH			
7″				137.9, CH			
11	-OCOCH$_3$	-OCOCH$_3$	-OCOCH$_3$	-OCOCH$_3$		-OCOCH$_3$	
1‴	170.9, C	171.1, C	170.8, C	170.8, C		171.1, C	
2‴	20.8, CH$_3$	20.9, CH$_3$	21.1, CH$_3$	21.1, CH$_3$		21.0, CH$_3$	

(d, J = 7.8 Hz, H-5′); δc 166.2 (C-1′), 130.0 (C-2′), 129.4 (C-3′ and C-7′), 128.4 (C-4′ and C-6′), and 133.2 (C-5′)] and a nicotinoyloxy function [$\delta$$_H$ 9.05 (s, H-3″), 8.68, (d, J = 4.2 Hz, H-5″) 7.22 (d, J = 4.2 Hz, H-6″), and 8.05 (d, J = 4.2 Hz, H-7″); δc 164.5 (C-1″), 125.4 (C-2″), 150.5 (C-3″), 152.8 (C-5″), 123.5 (C-6″), and 137.9 (C-7″)] in C-6 and C-7, respectively, established by the key HMBC correlations from H-6 to C-1′ and H-7 to C-1″. Thus, the structure of 6 was (11S*)-11-acetoxy-6α-benzoyloxy-8β,14-dihydroxy-7β-nicotinoyloxy-*neo*-cleroda-3,13-dien-15,16-olide.

Scutebarbolide E (7) was assigned a molecular formula of C$_{34}$H$_{44}$O$_{11}$ based on its HRESIMS ion at m/z 651.2784 [M + Na]$^{+}$ (calcd 651.2776). A comparison of the 1D and 2D NMR spectra of 7 with those of 6 suggested the occurrence of a 7-(2-hydroxy-3-methyl) butyryloxy group [$\delta$$_H$ 3.73 (d, J = 7.2 Hz, H-2″), 1.93 (m, H-3″), 0.84 (d, J = 7.2 Hz, H-4″), and 0.71 (d, J = 7.2 Hz, H-5″); δc 173.8 (C-1″), 75.3 (C-2″), 29.3 (C-3″), 19.2 (C-4″), and 15.8 (C-5″)] in 7 instead of the nicotinoyloxy group in 6. This was verified by the ^{1}H–^{1}H COSY correlations of H$_3$-4″/H-3″/H$_3$-5″, and the key HMBC cross-peaks from H-3″ to C-1″, from H-2″ to C-1″, and from H-7 to C-1″. Thus, the structure of

7 was defined as (11S*)-11-acetoxy-6α-benzoyloxy-8β,14-dihydroxy-7β-(2-hydroxy- 3-methyl)butyryloxy-*neo*-cleroda-3,13-dien-15,16-olide.

The HRESIMS data (m/z 556.2903 [M + H]$^{+}$ calcd 556.2905) of scutebarbolide F (8) showed a molecular formula of C$_{31}$H$_{41}$NO$_8$. The structure of 8 resembled that of scutolide J (4) (Wu et al., 2015) also isolated, except for the absence of the 11-acetoxy function and a 7-(2-hydroxy-3-methyl)butyryloxy substituent instead of the nicotinoyloxy group, as indicated by HMBC correlations from H-7 to C-1″. The ^{1}H–^{1}H COSY, HSQC, HMBC, and NOESY data further confirmed that the structure of 8 was defined as 8β-hydroxy-7β-(2-hydroxy-3-methyl)butyryloxy-6α-nicotinoyloxy-*neo*-cleroda-3,13-dien- 15,16-olide.

The HRESIMS (m/z 357.2036, [M + Na]$^{+}$, calcd 357.2036) and ^{13}C NMR data of scutebarbolide G (9) exhibited a molecular formula of C$_{20}$H$_{30}$O$_4$. A comparison of its NMR data with those of 1 revealed the absence of acyl substituents and the occurrence of two oxygenated methines and a secondary methyl in 9. The chemical shifts of C-6 (80.5), C-7 (74.6), and C-17 (11.2), the correlations of H-6/H-7/H-8/H$_3$-17 in the ^{1}H–^{1}H COSY spectrum, and the HMBC cross-peaks from H-
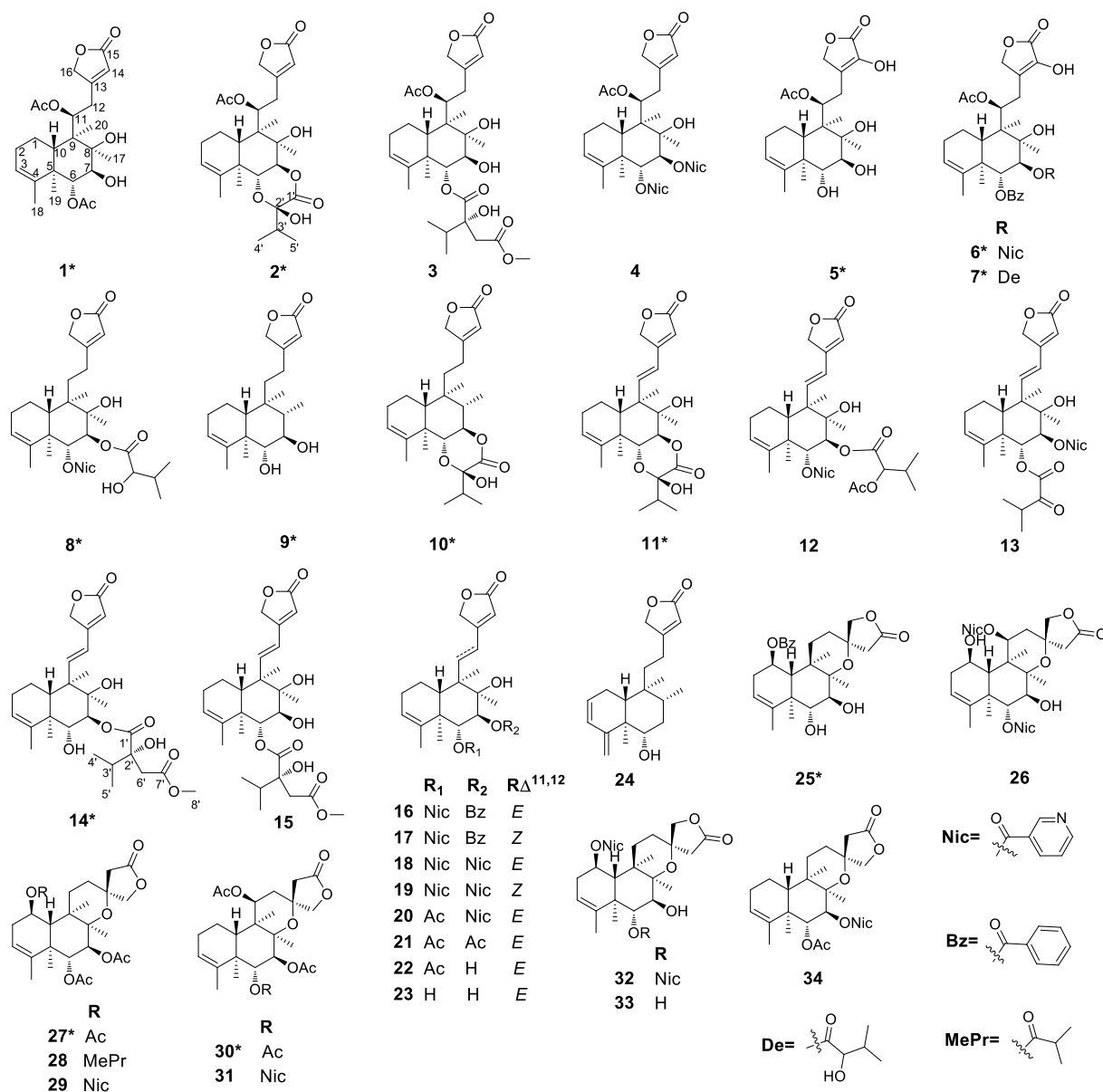
Fig. 1. Structures of compounds **1–34**.

6 to C-4 and C-5 and from H-7 to C-5, C-8, and C-17 established C-6 and C-7 as the oxygenated methines and C-17 as the secondary methyl. Thus, the structure of **9** was defined as 6α,7β-dihydroxy-*neo*-cleroda-3,13-dien-15,16-olide.

The molecular formula of scutebarbolide H (**10**) was assigned as $C_{25}H_{36}O_6$ according to the HRESIMS ion at *m/z* 455.2397 [M + Na]$^+$. Comparing the 1D NMR data (Tables 2 and 4) of **10** with those of **9** indicated the presence of the [6α(2′),7β(1′)-(2β-hydroxy-3-methylbutyryl)dioxy] group described above in **2** and displaying the same correlations. Thus, the structure of **10** was defined as 6α(2′),7β(1′)-(2β-hydroxy-3-methylbutyryl)dioxy-*neo*-cleroda-3,13-dien-15,16-olide.

Scutebarbolide I (**11**) displayed the molecular formula of $C_{25}H_{34}O_7$ based on the HRESIMS ion at *m/z* 447.2374 (calcd 447.2377, [M + H]$^+$) and ^{13}C NMR data, indicating that it had nine IOHDs. The NMR data of **11** (Tables 2 and 4) showed a close structural relationship with **2**: one additional double bond (**11**) replaced the 11-OAc, which was verified by the chemical shifts of H-11/C-11 (δ_H/δ_C 6.32/146.6) and H-12/C-12 (δ_H/δ_C 6.45/122.2), the ^1H–^1H COSY correlation of H-11/H-12, and the HMBC correlations from H-11 to C-10, C-20, and C-13 and from H-12 to C-13, C-14, and C-16. The observed $J_{11,12}$ value of 16.8 Hz

indicated that the Δ^{11} double bond was undisputedly assigned as an *E*-configuration. Thus, the structure of **11** was (11*E*)-8β-hydroxy-6α(2′),7β(1′)-(2β-hydroxy-3-methylbutyryl)dioxy-*neo*-cleroda-3,11,13-trien-15,16-olide.

Scutebarbolide J (**14**) possessed the molecular formula of $C_{28}H_{40}O_9$, as established by the HRESIMS data (*m/z* 543.2561 [M + Na]$^+$ calcd for $C_{28}H_{40}O_9Na$, 543.2565). A comparison of the 1D NMR data (Tables 2 and 4) of **14** with those of scutebata K (**15**) (Zhu et al., 2011), revealed their close structural relationship: the substituents 6 and 7 were exchanged. The hydroxyl group and 2′-hydroxy-2′-methoxycarbonylmethyl-3′-methylbutyroyloxy group were located at C-6 and C-7, respectively, as derived from the ^{13}C NMR resonance at δc 73.9 (C-7), the ^1H–^1H COSY correlation between H-6 and H-7, and the key HMBC cross-peak from H-6 to Me-19 and from H-7 to Me-17 and C-1′. The observed $J_{11,12}$ value of 16.8 Hz indicated the *E*-configuration of Δ^{11}. Thus, the structure of **14** was defined as (11*E*)-6α,8β-dihydroxy-7β-(2-hydroxy-2-methoxycarbonylmethyl-3-methyl)butyroyloxy-*neo*-cleroda-3,11,13-trien-15,16-olide.

Scutebarbolide K (**25**) was isolated as a white, amorphous powder, exhibiting a molecular formula of $C_{27}H_{34}O_7$ by the HRESIMS data (*m/z*
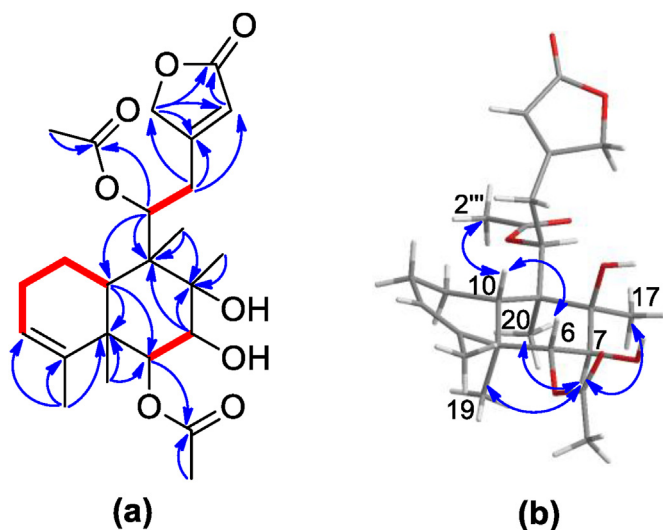
Fig. 2. (a) HMBC and ^1H–^1H COSY (b) NOESY correlations of compound **1**.

493.2195 [M + Na]$^+$ calcd 493.2197) and 1D NMR data (Tables 2 and 4). The 1D NMR spectra exhibited characteristic signals for 13-spiro-*neo*-clerodane-15,16-lactone skeleton (Zhu et al., 2011) also present in

other isolates (**25–34**). Besides, its ^1H and ^{13}C NMR spectra showed signals for three oxygenated methine signals [δ_H 5.13 (dd, J = 13.2 and 6.0 Hz), 3.66 (d, J = 9.0 Hz), and 3.44 (d, J = 9.0 Hz); δc 71.9, 74.5, and 76.4)] and one benzoyloxy group [δ_H 7.97 (d, J = 7.8 Hz, H-3′ and H-7′), 7.60, (t, J = 7.8 Hz, H-5′), and 7.47 (d, J = 7.8 Hz, H-4′ and H-6′); δc 165.8 (C-1′), 130.3 (C-2′), 128.7 (C-3′ and C-7′), 129.6 (C-4′ and C-6′), 133.4 (C-5′)]. The HMBC correlations from H-1 to C-1′, from H-6 to C-4, C-5, C-8, and C-10, and from H-7 to C-8 and C-9, as well as the ^1H–^1H COSY signal (Fig. 4a) between H-6 and H-7 established the benzoyloxy group attached at C-1 and two hydroxyl groups to C-6 and C-7.

The relative configuration of **25** was confirmed by the NOESY data (Fig. 4b). The H-1 was α-oriented based on the NOESY correlations of H-1/Me-19 and Me-20. The NOESY signals of H$_2$-14/Me-17 and H$_2$-12/H$_2$-16 implied the 13R* configuration assignment. Thus, the structure of **25** was (13R*)-1β-benzoyloxy-6α,7β-dihydroxy-8β,13-epoxy-*neo*-cleroda-3-en-15,16-olide.

Scutebarbolide L (**27**) was obtained as colorless crystals and scutebarbolide M (**30**) was isolated as yellow oil. These two compounds possessed a molecular formula of $C_{26}H_{36}O_9$ based on their HRESIMS data [m/z 515.2246 (**27**) and 515.2250 (**30**), [M + Na]$^+$, calcd 515.2252]. The 1D NMR spectra (Tables 2 and 4) of **27** and **30** suggested that they both shared a 13-spiro-15,16-lactone skeleton as **25**. Furthermore, the NMR data showed resonances for both compounds

Table 4
^{13}C NMR spectroscopic data of compounds **10**, **11**, **14**, **25**, **27**, and **30** (δ in ppm, in CDCl$_3$).

position	10[a]	11[b]	14[b]	25[a]	27[a]	30[b]
1	17.7, CH$_2$	19.2, CH$_2$	19.5, CH$_2$	71.9, CH	70.8, CH	17.9, CH$_2$
2	26.4, CH$_2$	26.3, CH$_2$	26.4, CH$_2$	32.9, CH$_2$	32.6, CH$_2$	26.3, CH$_2$
3	122.3, CH	122.3, CH	122.2, CH	118.9, CH	120.2, CH	123.4, CH
4	142.6, C	142.1, C	142.9, C	146.0, C	143.7, C	141.0, C
5	42.7, C	42.8, C	43.7, C	44.2, C	44.0, C	43.0, C
6	76.3, CH	72.3, CH	73.9, CH	74.5, CH	73.2, CH	74.1, CH
7	83.2, CH	83.8, CH	80.7, CH	76.4, CH	74.1, CH	74.4, CH
8	39.6, CH	76.0, C	76.5, C	81.4, C	80.7, C	83.1, C
9	39.3, C	48.2, C	48.6, C	38.6, C	38.7, C	43.2, C
10	45.1, CH	42.5, CH	42.4, CH	43.3, CH	43.3, CH	40.1, CH
11	35.3, CH$_2$	146.6, CH	147.8, CH	28.5, CH$_2$	28.5, CH$_2$	73.2, CH
12	22.0, CH$_2$	122.2, CH	121.7, CH	29.3, CH$_2$	29.2, CH$_2$	35.2, CH$_2$
13	170.0, C	162.3, C	162.5, C	76.3, C	76.6, C	77.1, C
14	115.4, CH	115.1, CH	114.7, CH	42.3, CH$_2$	44.3, CH$_2$	43.8, CH$_2$
15	174.0, C	174.3, C	173.6, C	174.8, C	173.9, C	173.2, C
16	73.2, CH$_2$	70.9, CH$_2$	70.9, CH$_2$	79.8, CH$_2$	76.4, CH$_2$	78.0, CH$_2$
17	10.1, CH$_3$	21.3, CH$_3$	23.0, CH$_3$	20.8, CH$_3$	19.8, CH$_3$	19.6, CH$_3$
18	21.9, CH$_3$	21.7, CH$_3$	22.4, CH$_3$	21.7, CH$_3$	20.0, CH$_3$	20.5, CH$_3$
19	16.8, CH$_3$	16.6, CH$_3$	16.4, CH$_3$	15.2, CH$_3$	16.4, CH$_3$	17.4, CH$_3$
20	19.0, CH$_3$	15.6, CH$_3$	15.5, CH$_3$	21.8, CH$_3$	20.9, CH$_3$	16.7, CH$_3$
					-OCOCH$_3$	-OCOCH$_3$
1′	170.7, C	170.7, C	174.5, C	165.8, C	170.2, C	170.5, C
2′	99.4, C	99.4, C	78.7, C	130.3, C	21.5, CH$_3$	21.7, CH$_3$
3′	36.8, CH	36.8, CH	35.9, CH	128.7, CH		
4′	14.4, CH$_3$	14.4, CH$_3$	17.4, CH$_3$	129.6, CH		
5′	17.2, CH$_3$	17.2, CH$_3$	16.9, CH$_3$	133.4, CH		
6′			41.1, CH$_2$	129.6, CH		
7′			173.6, C	128.7, CH		
8′			52.7, OCH$_3$			
					-OCOCH$_3$	-OCOCH$_3$
1″					169.9, C	171.0, C
2″					21.2, CH$_3$	21.0, CH$_3$
					-OCOCH$_3$	-OCOCH$_3$
1‴					171.0, C	170.2, C
2‴					21.6, CH$_3$	21.4, CH$_3$

^{c}Data were recorded at 75 MHz.
  ^{a} Data were recorded at 150 MHz.
  ^{b} Data were recorded at 100 MHz.
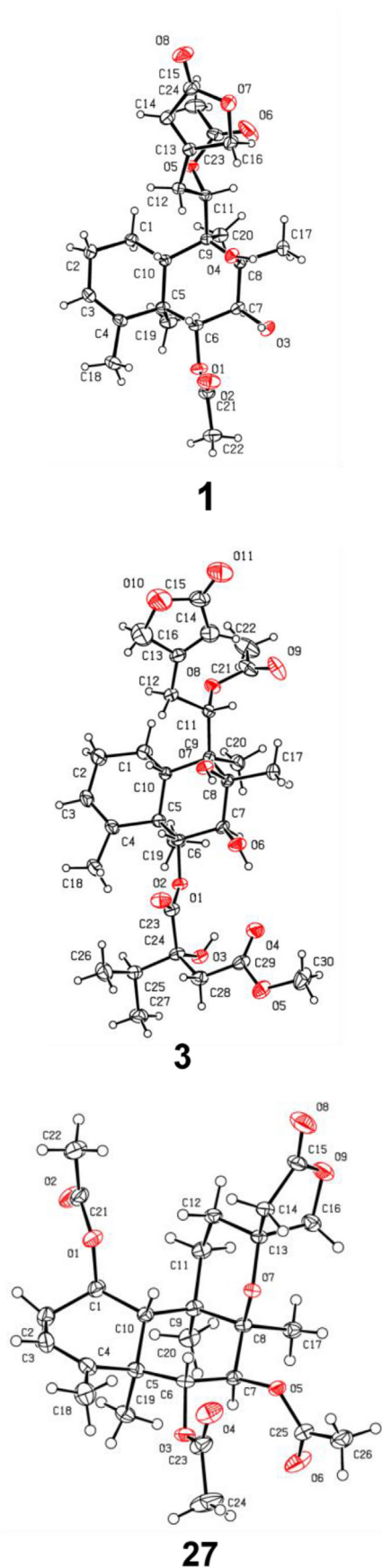
Fig. 3. ORTEP drawing of **1**, **3**, and **27**.
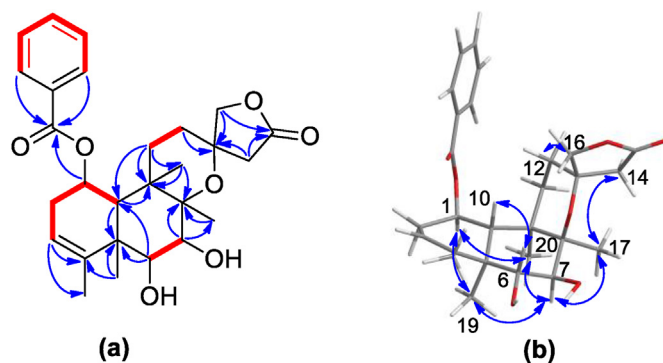
Fig. 4. (a) HMBC and ^{1}H–^{1}H COSY (b) NOESY correlations of compound **25**.

bearing three acetyl groups, two of them linked to C-6 and C-7. The only difference occurred at the linkage site of the third: C-1 in **27** but C-11 for **30**, pointed out by the key HMBC correlations from H-1 to C-1′ (δc 170.2), H-6 to C-1″ (δc 169.9) and H-7 to C-1‴ (δc 171.0) in **27** and from H-11 to C-1′ (δc 170.5), H-6 to C-1″ (δc 171.0) and H-7 to C-1‴ (δc 171.2) in **30**. For both compounds, the NOESY signals of H$_2$-16/Me-17 and H$_2$-12/H$_2$-14 implied an S^* configuration at C-13. In addition, the crystal X-ray diffraction experiment (Cu Kα radiation) of **27**, fully determined the assignment of its absolute configuration as (1R,5R,6R,7S,8R,9R,10S,13S) with a Flack parameter of −0.11(12) (Flack and Bernardinelli, 1999). The structure of **27** was defined as (1R,5R,6R,7S,8R,9R,10S,13S)-1,6,7-triacetoxy-8,13-epoxy-*neo*-cleroda-3-en-15,16-olide, showing the same substitution pattern as scutebata E (**28**) (Zhu et al., 2010), and barbatine D (**29**) (Nguyen et al., 2009). The structure of **30** was assigned as (13S^*)-6α,7β,11β-triacetoxy-8β,13-epoxy-*neo*-cleroda-3-en-15,16-olide, or 13-*epi*-scubatine D (Yuan et al., 2017), and also the 6α-acetoxy analog (Nic→Ac) of barbatine A (**31**) (Nguyen et al., 2009).

The mass spectrometry (MS), NMR data, and optical rotations of compounds **3**, **4**, **12**, **13**, **15–24**, **26**, **28**, **29**, and **31–34** were consistent with those of the known compounds reported in the literature, and their structures were assigned as scutebata W (**3**) (Yang et al., 2017), scutolide J (**4**) (Wu et al., 2015), scutolide B (**12**) (Wu et al., 2015), 6-*O*-(2-oxo-3-methylbutyroyl)scutehenanine A (**13**) (Dai et al., 2009), scutebata K (**15**) (Zhu et al., 2011), scutebarbatine B (**16**) (Dai et al., 2006), scutebartine F (**17**) (Xue et al., 2016), scutebarbatine A (**18**) (Nguyen et al., 2009), scutebartine G (**19**) (Xue et al., 2016), 6-*O*-acetylscutehenanine A (**20**) (Dai et al., 2009), 6,7-di-*O*-acetylbarbatin A (**21**) (Dai et al., 2007), scutebata I (**22**) (Zhu et al., 2011), barbatin C (**23**) (Dai et al., 2006), scubatine A (**24**) (Yuan et al., 2017), scutebartine C (**26**) (Xue et al., 2016), scutebata E (**28**) (Zhu et al., 2010), barbatine C (**29**) (Nguyen et al., 2009), barbatine A (**31**) (Nguyen et al., 2009), 6-*O*-nicotinoylscutebarbatine G (**32**) (Wang et al., 2010), scutebarbatine G (**33**) (Wang et al., 2010), scutebata O (**34**) (Zhu et al., 2011).

2.2. Phytotoxic activity of crude extracts of the aerial parts of S. barbata

The MeOH crude extract of the aerial parts of *S. barbata* was evaluated for its phytotoxic activity against two different plant seedlings and the results revealed that it showed dose-dependent inhibition effects on the growth of the roots and shoots of *L. perenne* and *L. sativa* seedlings at the concentrations ranging from 50 to 400 μg/mL (Fig. 5). To further target the active component, the phytotoxic activity of the EtOAc and *n*-BuOH fractions were also tested. The EtOAc fraction showed stronger inhibitory effects on these two plant seedlings than the *n*-BuOH fraction at all the tested concentrations. It was further found that the inhibition effect of the EtOAc fraction on the roots was greater than on the shoots for these two tested plant seedlings. Thus, a phytochemical investigation of the EtOAc fraction was performed, leading
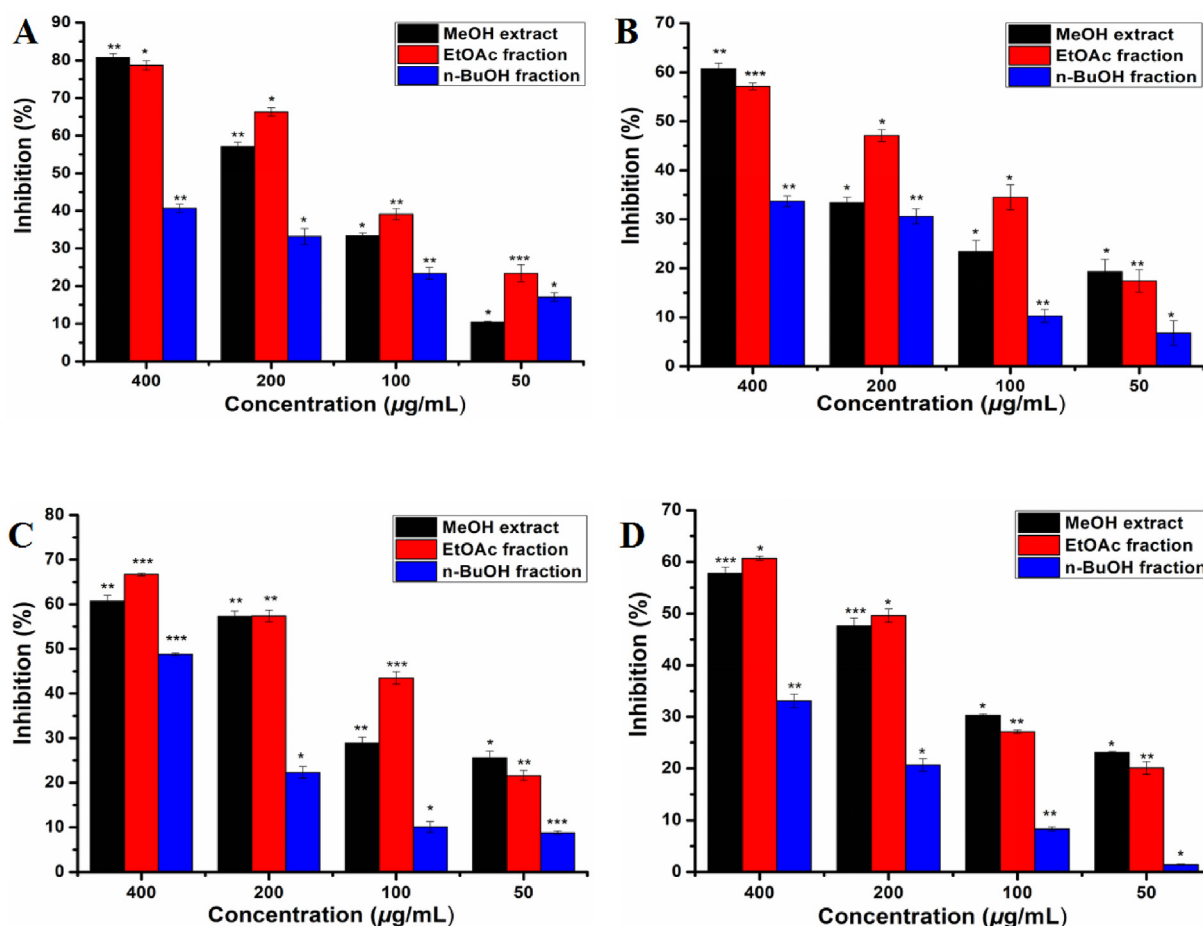
Fig. 5. Phytotoxic effects of the MeOH extract, the EtOAc fraction, and the n-BuOH fraction on the growth of the roots and shoots of *L. perenne* and *L. sativa* seedlings at concentrations of 400, 200, 100, 50 μg/mL, respectively. (A) *L. perenne* root, (B) *L. perenne* shoot, (C) *L. sativa* root, (D) *L. sativa* shoot. (*) $p < 0.05$, (**) $p < 0.01$, and (***) $p < 0.001$ versus the control group.

to the isolation of compounds **1–34**.

2.3. Phytotoxic activity of the purified compounds against L. Sativa and L. Perenne seedlings

The phytotoxic activity of compounds **1–34** against the growth of the roots and shoots of *L. perenne* and *L. sativa* seedlings were evaluated at a concentration of 200 μg/mL, with glyphosate as the positive control. All tested compounds displayed different degrees of inhibitory effects as shown in Table 5.

For the monocotyledon plant, *L. perenne*, compound **25** showed the most prominent inhibitory effects among all tested compounds, with its inhibition rate being 98.7% on the roots and 85.7% on the shoots, which was higher than the glyphosate (79.1% on the roots and 81.6% on the shoots). Compound **32** exhibited excellent inhibitory effects on the growth of roots with a inhibition rate of 96.2%. And compounds **2**, **3**, **15**, **18**, **20**, and **29** showed considerable inhibitory effects against the roots and shoots with the inhibition rates ranging from 63.0 to 84.7%, which were similar to those of glyphosate.

For the dicotyledon plant, *L. sativa*, compound **25** had significantly stronger inhibitory effects (98.0% on the roots and 89.3% on the shoots) than glyphosate (78.8% on the roots and 51.0% on the shoots). In addition, compounds **2**, **20**, **21**, **22**, and **27** showed good inhibitory effects on the roots with the inhibition rate ranging from 72 to 81% and on the shoots ranging from 50 to 70%, which were as active as glyphosate.

The phytotoxic activity of these compounds against the roots of the two tested plant seedlings was much stronger than against the shoots,

indicating that these compounds decreased seedling growth mainly by inhibiting the elongation of roots. When L. *perenne* and *L. sativa* seedlings were treated with **25** at a concentration of 200 μg/mL, wilting symptoms appeared on and finally death of these two tested plant seedlings.

2.4. Phytotoxic activity of compounds 2, 3, 15, 18, 25, 29, and 32 on L. Perenne seedlings at different concentrations

The inhibitory effects of compounds **2**, **3**, **15**, **18**, **25**, **29**, and **32** on the growth of the roots and shoots of *L. perenne* seedlings at different concentrations (25, 50, 100, and 200 μg/mL) were tested. All tested compounds obviously inhibited the growth of *L. perenne* seedlings in a dose-dependent manner (Fig. 6). As shown in Fig. 6A, compound **25** showed an inhibitory activity similar to that of glyphosate at low concentrations (25, 50, and 100 μg/mL) on the roots of *L. perenne*. In addition, compounds **3**, **18**, **20**, and **32** displayed moderate inhibitory effects with their inhibition rates ranging from 35 to 70% at low concentrations. In Fig. 6B, compound **25** displayed much higher inhibitory effects on the shoots of *L. perenne* than glyphosate at all tested concentrations (from 25 to 200 μg/mL), while the inhibitory effects of other compounds (**2**, **3**, **15**, **18**, **29**, and **32**) were similar to those of glyphosate at low concentrations.

2.5. Phytotoxic activity of compounds 2, 20, 21, 22, 25, and 27 on L. Sativa seedlings at different concentrations

The inhibitory effects of compounds **2**, **20**, **21**, **22**, **25**, and **27** on the

Table 5
Inhibitory effects of compounds **1–34** on the growth of the roots and shoots of *L. sativa* and *L. perenne* seedlings.[a]

compound	inhibition rates (%)[b]			
	L. perenne		L. sativa	
	root	shoot	root	shoot
1	32.8 ± 1.9**	25.4 ± 2.8*	45.3 ± 0.9***	33.3 ± 1.6**
2	84.7 ± 1.6***	63.0 ± 2.3**	81.2 ± 2.0***	56.1 ± 3.8**
3	82.2 ± 0.2***	72.1 ± 2.1**	51.4 ± 1.2**	41.8 ± 1.5**
4	53.9 ± 0.5**	38.5 ± 0.4***	47.1 ± 1.5*	20.4 ± 1.6
5	50.0 ± 1.2*	42.8 ± 1.4*	25.4 ± 1.9*	33.6 ± 1.6
6	50.0 ± 1.2*	40.8 ± 1.4*	35.5 ± 2.9	23.2 ± 1.8
7	23.3 ± 1.5*	5.7 ± 1.3	10.3 ± 1.1	6.4 ± 0.3*
8	66.5 ± 0.5***	36.5 ± 3.9	13.6 ± 1.2	11.9 ± 1.2
9	13.3 ± 1.5*	15.9 ± 1.3	3.3 ± 1.5*	14.9 ± 1.6
10	65.1 ± 1.8**	32.2 ± 0.7	16.3 ± 1.3	10.7 ± 1.2**
11	56.1 ± 1.5**	42.2 ± 1.7*	34.4 ± 2.2*	23.1 ± 2.3*
12	33.3 ± 1.8	15.7 ± 2.3	14.3 ± 1.4*	18.7 ± 1.5*
13	60.8 ± 0.7*	55.4 ± 1.5*	9.6 ± 1.4	3.3 ± 1.5
14	46.2 ± 1.3*	40.2 ± 0.1**	30.6 ± 1.4	21.5 ± 1.1*
15	87.3 ± 0.4***	73.1 ± 0.6***	10.3 ± 1.3*	8.7 ± 1.7*
16	50.0 ± 1.4	28.5 ± 1.5	18.5 ± 1.8**	10.9 ± 1.2**
17	17.2 ± 1.5*	18.0 ± 0.1*	38.2 ± 2.5	31.4 ± 0.9**
18	83.3 ± 0.4***	66.4 ± 0.2***	50.3 ± 2.7*	53.1 ± 1.3
19	17.4 ± 0.7	13.8 ± 0.2	9.8 ± 1.1	10.1 ± 2.4
20	85.4 ± 1.5***	77.9 ± 0.3**	80.7 ± 3.5*	57.6 ± 3.4*
21	52.9 ± 1.9**	37.6 ± 0.7	73.3 ± 2.3***	70.2 ± 2.4*
22	47.7 ± 2.2**	14.9 ± 1.7	72.9 ± 0.8***	66.2 ± 0.3***
23	13.9 ± 1.1	6.7 ± 1.6	40.8 ± 2.8*	37.2 ± 1.2**
24	65.1 ± 1.3***	23.5 ± 3.0	24.3 ± 1.4*	26.1 ± 1.6*
25	98.7 ± 0.2***	85.7 ± 0.3***	98.0 ± 1.1***	89.3 ± 1.2**
26	22.8 ± 1.0*	24.3 ± 1.1**	25.2 ± 2.3	39.2 ± 2.7*
27	42.1 ± 3.9*	32.5 ± 5.7	67.7 ± 2.3**	49.7 ± 0.4*
28	39.5 ± 1.4**	53.9 ± 1.1	58.0 ± 1.5***	34.0 ± 1.1**
29	86.7 ± 1.5***	73.5 ± 0.3***	30.2 ± 1.4*	24.7 ± 1.1
30	56.7 ± 1.7**	37.9 ± 1.3	26.7 ± 1.8**	17.9 ± 1.2
31	59.1 ± 1.0***	38.1 ± 1.1*	36.1 ± 0.7**	35.3 ± 2.7
32	96.2 ± 0.3***	76.5 ± 1.0**	58.9 ± 3.2*	50.6 ± 1.2
33	45.1 ± 0.1**	43.6 ± 2.7	34.6 ± 0.7**	23.7 ± 2.7**
34	56.1 ± 1.5**	42.2 ± 1.7*	34.4 ± 2.2*	23.1 ± 2.3*
glyphosate	79.3 ± 1.0***	81.6 ± 1.6***	78.8 ± 1.5**	51.0 ± 1.5**

(*) p < 0.05, (**) p < 0.01, and (***) p < 0.001 versus the control group.
[a] All the compounds were tested at a concentration of 200 μg/mL.
[b] Values were presented as a percentage of the mean compared to the control (mean ± SD).

growth of the roots and shoots of *L. sativa* seedlings at different concentrations (25, 50, 100, and 200 μg/mL) were also evaluated. At low concentrations (25, 50, and 100 μg/mL), compound **25** showed inhibitory effects on the roots similar to glyphosate, while other compounds exhibited weak inhibitory effects (Fig. 7A). As shown in Fig. 7B, all tested compounds exhibited stronger inhibitory effects on the shoots than glyphosate, especially compounds **21**, **22**, and **25**.
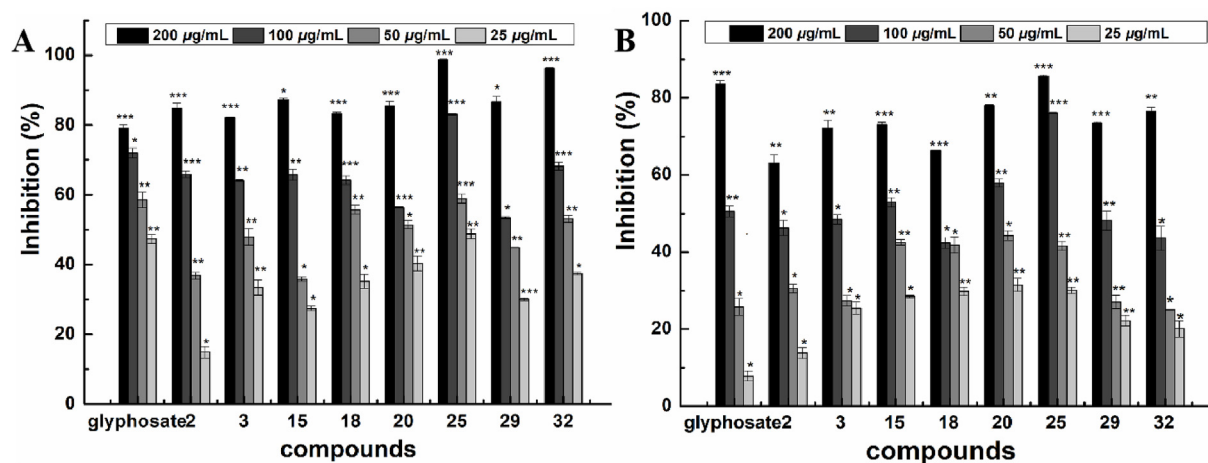

Fig. 6. Phytotoxic effects of compound **2**, **3**, **15**, **18**, **20**, **25**, **29**, **32**, and glyphosate (positive control) on the growth of the roots and shoots of *L. perenne* seedlings at concentrations of 200, 100, 50, 25 μg/mL, respectively. (A) *L. perenne* root, (B) *L. perenne* shoot. (*) p < 0.05, (**) p < 0.01, and (***) p < 0.001 versus the control group.
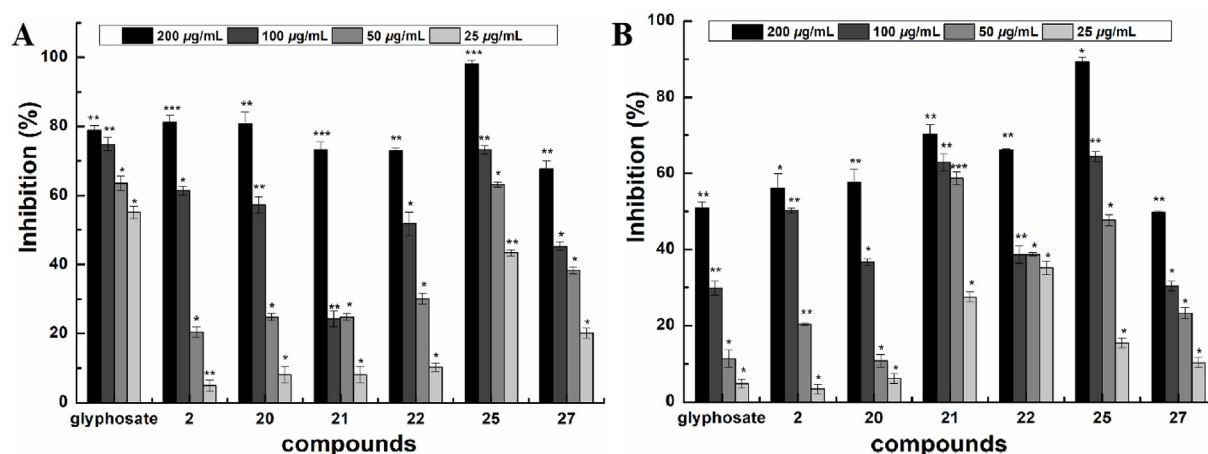
Fig. 7. Phytotoxic effects of compound **2**, **20**, **21**, **22**, **25**, **27**, and glyphosate (positive control) on the growth of the roots and shoots of *L. sativa* seedlings at concentrations of 200, 100, 50, 25 μg/mL, respectively. (A) *L. sativa* shoot, (B) *L. sativa* root. (*) $p < 0.05$, (**) $p < 0.01$, and (***) $p < 0.001$ versus the control group.

2.6. A structure-activity relationship analysis of the purified compounds

For the monocotyledon plant, *L. perenne*, compounds **2**, **10**, and **11** with a 6,7-dioxygen lactone system exhibited considerable activity, indicating that the 6,7-dioxygen lactone system might enhance the phytotoxic activity. Compounds **3** and **15** exhibited stronger inhibitory effects than compound **14**, which was attributed to the 2′-hydroxy-2′-methoxycarbonylmethyl-3′-methylbutyroyloxy at C-6 rather than at C-7. The inhibitory effect of **16** was better than that of **17** and the inhibitory effect of **18** was superior to that of **19**, which suggested that the Δ^{11} double bond as an *E*-configuration were more favorable to their phytotoxic activity. Compound **25** showed the best inhibitory effect compared with compounds **26–34**, which was attributed to the *R**-configuration of C-13, along with the benzoyloxy group at C-1. Correspondingly, the brilliant inhibitory effects of **32** might be assigned to two nicotinoyloxy groups.

For the dicotyledon plant, *L. sativa*, a common acetyl group attached at C-6 in compounds **20**, **21**, and **22** was vital for their phytotoxic activity compared with compound **23**. Compound **25** exhibited the best phytotoxic activity among compounds **25–34**, which suggested that the *R**-configuration of C-13 and the benzoyloxy group at C-1 might have played a significant role in its phytotoxic activity.

3. Conclusion

In this study, our findings demonstrated that the *neo*-clerodane diterpenoids from the aerial parts of *S. barbata*, exhibited potent phytotoxic activity. Notably, the inhibitory effects of compound **25** against the growth of the roots and shoots of *L. perenne* and *L. sativa* seedlings were as active as the positive control at all tested concentrations (25, 50, 100, and 200 μg/mL). Moreover, when these two tested plant seedlings were treated with **25** at 200 μg/mL, plant seedlings showed symptoms of wilting and death. Thus, *neo*-clerodane diterpenoids from *S. barbata*, especially compound **25**, could be promising lead compounds for the development of renewable and environmentally friendly herbicides that are less harmful to wildlife and human beings.

4. Experimental

4.1. General experimental procedures

The infrared (IR) spectra were recorded on using a Bruker Tensor 27 spectrometer. The ultraviolet (UV) spectra were measured on a Shimadzu UV-260 spectrophotometer. A PerkinElmer model 341 polarimeter was used for measuring optical rotations. High-resolution electrospray ionization mass spectrometry (HRESIMS) was recorded by a Bruker Daltonics APEX II spectrometer. X-ray crystallography was collected on a Bruker Smart charge-coupled device (CCD) diffractometer (Bruker, Ltd., Karlsruhe, Germany) using graphic-mono-chromated Cu K*α* radiation. ^{1}H and ^{13}C nuclear magnetic resonance (NMR) spectra were acquired on a Varian Mercury-600BB or a Bruker AVANCE III-400 spectrometer with tetramethylsilane (TMS) as an internal standard. Semi-preparative high-performance liquid chromatography (HPLC) was conducted on a Waters equipment (1525 pump and 2998 photodiode array detector) with a SunFre Prep C$_{18}$ column (150 × 10 mm, 10 μm, with a flow rate of 2 mL/min). LiChroprep RP-C$_{18}$ gel (40–63 μm, Merck, Germany) and Sephadex LH-20 were purchased from Amersham Pharmacia Biotech. Silica gel (200–300 mesh) used for column chromatography and silica GF254 (10–40 mm) used for thin-layer chromatography (TLC) were both supplied by the Qingdao Marine Chemical Factory, Qingdao, People's Republic of China.

4.2. Plant materials

The aerial parts of *S. barbata* D. Don were collected in Queshan County, Henan Province, China, in August 2018 and identified by Li Jianyin, a professor in Lanzhou University. A voucher specimen (no. Sb2018820) was stored at the Natural Product Laboratory of the State Key Laboratory of Applied Organic Chemistry, Lanzhou University.

4.3. Extraction, isolation, and purification process

The collected aerial parts of *S. barbata* were dried in shade and pulverized to give a 10 kg plant sample. It was soaked in 80 L methanol at room temperature for 3 times, 7 days each time. All extracts were combined and condensed to yield a crude extract (1 kg), which was dissolved in hot distilled water and extracted with ethyl acetate and *n*-butanol, successively.

The ethyl acetate extract (200 g) was chromatographed over macroporous resin, eluted with gradient systems of methanol/water (30:70, 50:50, 80:20, 95:5, *v:v*) to give four parts (30%, 50%, 80%, and 95%). Part 80% (50 g) was chromatographed on a MCI column with a gradient of ethanol/water (60:40, 70:30, 80:20, 90:10, 100:0, *v:v*) as the eluent, then five fractions (A − E) were collected according to TLC analysis. Fraction B (10 g) was applied to a silica gel column (10:1, 8:1, 5:1, 3:1, 1:1, *v:v*, petroleum ether/acetone) to afford four samples (B1–B4). Compounds **8** (8 mg), **12** (20 mg), and **13** (25 mg) were obtained from fraction B1 (0.9 g) by a reversed-phase column (from 60:40 to 100:0, *v:v*, MeOH/H$_2$O). Fraction B2 (5 g) was separated on a Sephadex LH-20

column (MeOH:CH$_2$Cl$_2$, 1:1, *v:v*) to obtain three fractions (B21–B23). Fraction B22 (200 mg) was further purified by semi-preparative HPLC to obtain compounds **4** (15 mg, t$_R$ = 18 min), **25** (20 mg, t$_R$ = 20 min), and **26** (8 mg, t$_R$ = 13 min). Compounds **16** (40 mg, t$_R$ = 41 min), **17** (50 mg, t$_R$ = 39 min), **18** (95 mg, t$_R$ = 11 min), and **19** (89 mg, t$_R$ = 14 min) were collected from fraction B23 (600 mg) over semi-preparative HPLC chromatography, eluted with MeCN/H$_2$O (3:2, *v:v*, 2 mL/min). Fraction B3 (2 g) was subjected to a Sephadex LH-20 column with MeOH as the eluent and further purified by a silica gel column (8:1, 5:1, 3:1, 1:1, *v:v*, CH$_2$Cl$_2$/EtOAc) to give compounds **6** (5 mg), **29** (33 mg), and **32** (20 mg). Fraction B4 (400 mg) was applied to semi-preparative HPLC (MeCN/H$_2$O, 3:2, *v:v*, 2 mL/min) to afford compounds **31** (30 mg, t$_R$ = 17 min), **33** (12 mg, t$_R$ = 10 min), and **34** (5 mg, t$_R$ = 28 min). Fraction C (15 g) was loaded on a silica gel column (10:1, 8:1, 5:1, 3:1, 1:1, *v:v*, Petroleum ether/Ethyl acetate) to collect four samples (C1–C4). Fraction C1 (2 g) was chromatographed on Sephadex LH-20 chromatography (MeOH) and further purified by a reversed-phase column chromatography (from 50:50 to 100:0, *v:v*, MeCN/H$_2$O) to obtain compounds **1** (20 mg), **2** (17 mg), **9** (6 mg), and **24** (34 mg). Fraction C2 (1.3 g) was separated on Sephadex LH-20 chromatography (MeOH) and further purified by a reversed-phase column chromatography (from 50:50 to 100:0, *v:v*, MeCN/H$_2$O) to give compounds **3** (30 mg), **14** (10 mg), and **15** (30 mg). Fraction C3 (8 g) was segmented by a Sephadex LH-20 chromatography (MeOH) to yield three fractions (C31–C33). Fraction C31 (2 g) was applied to a silica gel column (10:1, 5:1, 3:1, 1:1, *v:v*, CH$_2$Cl$_2$/EtOAc) to afford compounds **5** (20 mg), **7** (13 mg), and **13** (30 mg). Compounds **20** (25 mg, t$_R$ = 28 min), **21** (30 mg, t$_R$ = 18 min), **22** (18 mg, t$_R$ = 20 min), and **23** (25 mg, t$_R$ = 11 min) were obtained from fractions C32 (600 mg) by the semi-preparative HPLC (MeCN/H$_2$O, 3:1, *v:v*, 2 mL/min). Fraction C33 (1 g) was further purified on a Sephadex LH-20 (MeOH) and a reversed-phase column chromatography (from 50:50 to 100:0, *v:v*, MeOH/H$_2$O) to give compounds **8** (16 mg), **10** (13 mg), **11** (6 mg), and **12** (30 mg). Compounds **27** (4 mg, t$_R$ = 45 min), **28** (10 mg, t$_R$ = 53 min), and **30** (8 mg, t$_R$ = 18 min) were isolated from fraction C4 (80 mg) by the semi-preparative HPLC (MeCN/H$_2$O, 3:1, *v:v*, 2 mL/min).

Scutebarbolide A (1): colorless needles (acetone); [α]19 D = −41.9 (*c* 0.8, MeOH); UV (MeOH) λ$_{max}$ (log ε) 260 (0.46), 207 (0.81) nm; IR (KBr) ν$_{max}$ 3456, 2982, 2929, 1780, 1739, 1640, 1373, 1239 cm^{-1}; ^{1}H and ^{13}C NMR data, see Tables 1 and 3; HRESIMS *m/z*: [M + H]$^+$ calcd for C$_{24}$H$_{34}$O$_8$H, 451.2326; found, 451.2333.

Scutebarbolide B (2): white, amorphous solids; [α]19 D = −15.2 (*c* 0.1, MeOH); UV (MeOH) λ$_{max}$ (log ε) 257 (0.21), 207 (0.36) nm; IR (KBr) ν$_{max}$ 3367, 2925, 2865, 1746, 1598, 1459, 1248 cm^{-1}; ^{1}H and ^{13}C NMR data, see Tables 1 and 3; HRESIMS *m/z*: [M + Na]$^+$ calcd for C$_{27}$H$_{38}$O$_9$Na 529.2408; found, 529.2408.

Scutebarbolide C (5): yellow oil; [α]19 D = −27.4 (*c* 0.3, MeOH); UV (MeOH) λ$_{max}$ (log ε) 257 (0.04), 211 (0.22) nm; IR (KBr) ν$_{max}$ 3438, 2983, 2833, 1736, 1654, 1373, 1239, 1133 cm^{-1}; ^{1}H and ^{13}C NMR data, see Tables 1 and 3; HRESIMS *m/z*: [M + H]$^+$ calcd for C$_{22}$H$_{33}$O$_8$ 425.2170; found, 425.2176.

Scutebarbolide D (6): white, amorphous solids; [α]19 D = −28.0 (*c* 0.2, MeOH); UV (MeOH) λ$_{max}$ (log ε) 260 (0.24), 216 (0.19) nm; IR (KBr) ν$_{max}$ 3413, 2982, 1731, 1655, 1509, 1450, 1239 cm^{-1}; ^{1}H and ^{13}C NMR data, see Tables 1 and 3; HRESIMS *m/z*: [M + H]$^+$ calcd for C$_{35}$H$_{40}$NO$_{10}$ 634.2647; found, 634.2664.

Scutebarbolide E (7): white, amorphous solids; [α]19 D = −20.0 (*c* 0.1, MeOH); UV (MeOH) λ$_{max}$ (log ε) 278 (0.17), 230 (1.35) nm; IR (KBr) ν$_{max}$ 3435, 2973, 2932, 1778, 1732, 1449, 1283 cm^{-1}; ^{1}H and ^{13}C NMR data, see Tables 1 and 3; HRESIMS *m/z*: [M + Na]$^+$ calcd for C$_{34}$H$_{44}$O$_{11}$Na 651.2776; found, 651.2784.

Scutebarbolide F (8): yellow oil; [α]19 D = −21.2 (*c* 0.3, MeOH); UV (MeOH) λ$_{max}$ (log ε) 262 (0.25), 211 (1.09) nm; IR (KBr) ν$_{max}$ 3418, 2962, 2873, 1736, 1637, 1421, 1278 cm^{-1}; ^{1}H and ^{13}C NMR data, see Tables 1 and 3; HRESIMS *m/z*: [M + H]$^+$ calcd for C$_{31}$H$_{42}$NO$_8$

556.2905; found, 556.2903.

Scutebarbolide G (9): yellow oil; [α]19 D = −15.1 (*c* 0.1, MeOH); UV (MeOH) λ$_{max}$ (log ε) 261 (0.11), 210 (0.46) nm; IR (KBr) ν$_{max}$ 3418, 2929, 1779, 1744, 1638, 1444, 1267 cm^{-1}; ^{1}H and ^{13}C NMR data, see Tables 1 and 3; HRESIMS *m/z*: [M + Na]$^+$ calcd for C$_{20}$H$_{30}$O$_4$Na 357.2036; found, 357.2036.

Scutebarbolide H (10): white, amorphous solids; [α]19 D = −18.5 (*c* 0.5, MeOH); UV (MeOH) λ$_{max}$ (log ε) 253 (0.10), 207 (0.69) nm; IR (KBr) ν$_{max}$ 3440, 2968, 2934, 1780, 1745, 1468, 1387 cm^{-1}; ^{1}H and ^{13}C NMR data, see Tables 2 and 4; HRESIMS *m/z*: [M + Na]$^+$ calcd for C$_{25}$H$_{36}$O$_6$Na 455.2404; found, 455.2397.

Scutebarbolide I (11): white, amorphous solids; [α]19 D = −33.6 (*c* 0.2, MeOH); UV (MeOH) λ$_{max}$ (log ε) 257 (0.57) nm; IR (KBr) ν$_{max}$ 3433, 2963, 1778, 1744, 1644, 1239, 1136,1033 cm^{-1}; ^{1}H and ^{13}C NMR data, see Tables 2 and 4; HRESIMS *m/z*: [M + H]$^+$ calcd for C$_{25}$H$_{35}$O$_7$ 447.2377; found, 447.2374.

Scutebarbolide J (14): white, amorphous solids; [α]19 D = −19.8 (*c* 0.1, MeOH); UV (MeOH) λ$_{max}$ (log ε) 260 (0.12), 211 (0.29) nm; IR (KBr) ν$_{max}$ 3428, 2953, 2923, 1778, 1736, 1642, 1152 cm^{-1}; ^{1}H and ^{13}C NMR data, see Tables 2 and 4; HRESIMS *m/z*: [M + Na]$^+$ calcd for C$_{28}$H$_{40}$O$_9$Na 543.2565; found, 543.2561.

Scutebarbolide K (25): yellow oil; [α]19 D = −52.2 (*c* 0.4, MeOH); UV (MeOH) λ$_{max}$ (log ε) 260 (0.10), 229 (0.38) nm; IR (KBr) ν$_{max}$ 3485, 2958, 1780, 1739, 1712, 1275 cm^{-1}; ^{1}H and ^{13}C NMR data, see Tables 2 and 4; HRESIMS *m/z*: [M + Na]$^+$ calcd for C$_{27}$H$_{34}$O$_7$Na 493.2197; found, 493.2195.

Scutebarbolide L *(27)*: colorless needles (in MeOH); [α]19 D = −15.2 (*c* 0.1, MeOH); UV (MeOH) λ$_{max}$ (log ε) 267 (0.43) nm; IR (KBr) ν$_{max}$ 3444, 2976, 1787, 1747, 1374, 1242, 1026 cm^{-1}; ^{1}H and ^{13}C NMR data, see Tables 2 and 4; HRESIMS *m/z*: [M + Na]$^+$ calcd for C$_{26}$H$_{36}$O$_9$Na 515.2252; found, 515.2246.

Scutebarbolide M (30): yellow oil; [α]19 D = −15.2 (*c* 0.1, MeOH); UV (MeOH) λ$_{max}$ (log ε) 267 (0.42) nm; IR (KBr) ν$_{max}$ 3456, 2973, 1789, 1743, 1372, 1232, 1029 cm^{-1}; ^{1}H and ^{13}C NMR data, see Tables 2 and 4; HRESIMS *m/z*: [M + Na]$^+$ calcd for C$_{26}$H$_{36}$O$_9$Na 515.2252; found, 515.2250.

4.4. Crystallographic data of scutebarbolide A (1), scutebata W (3), Scutebarbolide L (27)

Crystal data for **1** (CCDC, 1940172), mp 200–203 °C; C$_{24}$H$_{34}$O$_8$, *M* = 450.51, *T* = 292.09(12) K, orthorhombic, space group P2$_1$2$_1$2$_1$, *a* = 12.5138(3) Å, *b* = 12.5380(3) Å, c = 14.6757(3) Å, α = 90.00°, β = 90.00°, γ = 90.00°, *V* = 2302.58(10) Å^3, *Z* = 4, μ(CuKα) = 0.801 mm^{-1}, *D*calc = 1.300 g/cm^3, single crystal size: 0.18 × 0.15 × 0.12 mm^3, 9369 reflections measured (9.278° ≤ 2Θ ≤ 133.022°), 3896 unique (*R*$_{int}$ = 0.0257, *R*$_{sigma}$ = 0.0312) which were used in all calculations. The final *R*$_1$ was 0.0378 (> 2σ(I)) and *wR*$_2$ was 0.0908 (all data), Flack parameter = 0.00(9).

Crystal data for **3** (CCDC, 1940171), mp 204–206 °C; C$_{30}$H$_{44}$O$_{11}$, *M* = 580.65, *T* = 292.39(10) K, orthorhombic, space group P2$_1$2$_1$2$_1$, *a* = 9.78236(18) Å, *b* = 10.04385(17) Å, c = 31.5204(5) Å, α = 90.00°, β = 90.00°, γ = 90.00°, *V* = 3096.96(9) Å^3, *Z* = 4, μ(CuKα) = 0.784 mm^{-1}, *D*calc = 1.245 g/cm^3, single crystal size: 0.18 × 0.15 × 0.12 mm^3, 11,092 reflections measured (9.242° ≤ 2Θ ≤ 133.162°), 5464 unique (*R*$_{int}$ = 0.0154, *R*$_{sigma}$ = 0.0196) which were used in all calculations. The final *R*$_1$ was 0.0458 (> 2σ(I)) and *wR*$_2$ was 0.1165 (all data), Flack parameter = 0.09(5).

Crystal data for **27** (CCDC, 1940170), mp 228–231 °C; C$_{26}$H$_{36}$O$_9$, *M* = 492.55, *T* = 140.00(10) K, orthorhombic, space group P2$_1$2$_1$2$_1$, *a* = 10.4120(5) Å, *b* = 10.9787(5) Å, c = 22.5852(11)Å, α = 90.00°, β = 90.00°, γ = 90.00°, *V* = 2581.7(2) Å^3, *Z* = 4, μ(CuKα) = 0.790 mm^{-1}, *D*calc = 1.267 g/cm^3, single crystal size: 0.18 × 0.15 × 0.12 mm^3, 8651 reflections measured

4.5. Phytotoxicity assay

Using glyphosate as the positive control, phytotoxic activity of these neo-clerodane diterpenoids on the growth of the roots and shoots of *L. sativa* and *L. perenne* seedlings were evaluated using published methods (Liu et al., 2017; Wei et al., 2018; Han et al., 2019; Yuan et al., 2014). The inhibition rates (%) were established using formula [1 − treated length/control length] × 100%.

4.6. Statistical analysis

All data presented were obtained from three independent experiments and were presented as the mean ± standard deviation (SD). Statistical analysis was performed using one-way analysis of variance (ANOVA). The mean values were compared using Student's *t*-test, and p values of < 0.05, < 0.01, and < 0.001 were denoted as ∗, ∗∗, and ∗∗∗, respectively.

Notes

The authors declare no competing financial interest.

Declaration of competing interest

We declare that we have no financial and personal relationships with other people or organizations that can inappropriately influence our work, there is no professional or other personal interest of any nature or kind in any product, service and/or company that could be construed as influencing the position presented in, or the review of, the manuscript entitled, "Phytotoxic neo-Clerodane Diterpenoids from the Aerial Parts of Scutellaria barbata".

Appendix A. Supplementary data

Supplementary data to this article can be found online at https://doi.org/10.1016/j.phytochem.2019.112230.

References

Bisio, A., Damonte, G., Fraternale, D., Giacomelli, E., Salis, A., Romussi, G., Cafaggi, S., Ricci, D., Tommasi, N.D., 2011. Phytotoxic clerodane diterpenes from *Salvia miniata* fernald (Lamiaceae). Phytochemistry 72, 265–275.

Dai, S.J., Tao, J.Y., Liu, K., Jiang, Y.T., Shen, L., 2006. *neo*-Clerodane diterpenoids from *Scutellaria barbata* with cytotoxic activities. Phytochemistry 67, 1326–1330.

Dai, S.J., Wang, G.F., Chen, M., Liu, K., Shen, L., 2007. Bioactive *ent*-clerodane diterpenoids from *Scutellaria barbata*. Planta Med. 73, 1217–1220.

Dai, S.J., Peng, W.B., Zhang, D.W., Shen, L., Wang, W.Y., Ren, Y., 2009. Cytotoxic *neo*-clerodane diterpenoid alkaloids from *Scutellaria barbata*. J. Nat. Prod. 72, 1793–1797.

Dai, S.J., Peng, W.B., Shen, L., Zhang, D.W., Ren, Y., 2011. New *nor*-diterpenoid alkaloids from *Scutellaria barbata* with cytotoxic activities. Nat. Prod. Res. 25, 1019–1024.

Flack, H.D., Bernardinelli, G., 1999. Absolute structure and absolute configuration. Acta Cryst. Sect. A55, 908–915.

Guo, F., Yang, F., Zhu, Y.H., 2019. Scutellarein from *Scutellaria barbata* induces apoptosis of human colon cancer HCT116 cells through the ROS-mediated mitochondria dependent pathway. Nat. Prod. Res. 33, 2372–2375.

Han, W.B., Zhai, Y.J., Gao, Y., Zhou, H.Y., Xiao, J., Pescitelli, G., Gao, J.M., 2019. Cytochalasins and an abietane-type diterpenoid with allelopathic activities from the endophytic fungus *Xylaria* species. J. Agric. Food Chem. 67, 3643–3650.

Li, J., Wang, Y., Lei, J.C., Hao, Y., Yang, Y., Yang, C.X., Yu, J.Q., 2014a. Sensitisation of ovarian cancer cells to cisplatin by flavonoids from *Scutellaria barbata*. Nat. Prod. Res. 28, 683–689.

Li, R.J., Sun, Y., Sun, B., Wang, X.N., Liu, S.S., Zhou, J.C., Ye, J.P., Zhao, Y., Liu, L., Lee, K.H., Lou, H.X., 2014b. Phytotoxic *cis*-clerodane diterpenoids from the Chinese liverwort *Scapania stephanii*. Phytochemistry 105, 85–91.

Liu, Q., Wu, C.H., Peng, A.F., Gao, K., Chen, J.J., Li, Y., Fu, H., 2017. Flavonolignans from *Elymus natans* L. and phytotoxic activities. J. Agric. Food Chem. 65, 1320–1327.

Macías, F.A., Castellano, D., Molinillo, J.M.G., 2000. Search for a standard phytotoxic bioassay for allelochemicals. selection of standard target species. J. Agric. Food Chem. 48, 2512–2521.

Nguyen, V.H., Pham, V.C., Nguyen, T.T.H., Tran, V.H., Doan, T.M.H., 2009. Novel antioxidant *neo*-clerodane diterpenoids from *Scutellaria barbata*. Eur. J. Org. Chem. 33, 5810–5815.

Owen, M.D.K., Zelaya, I.A., 2005. Herbicide-resistant crops and weed resistance to herbicides. Pest Manag. Sci. 61, 301–311.

Shaik, R.S., Burrows, G.E., Urwin, N.A.R., Gopurenko, D., Lepschi, B.J., Weston, L.A., 2017. The biology and management of prickly paddy melon (*Cucumis myriocarpus* L.), an important summer annual weed in Australia. Crop Protect. 92, 29–40.

Tshewang, S., Sindel, B.M., Ghimiray, M., Chauhan, B.S., 2016. Weed management challenges in rice (*Oryza sativa* L.) for food security in Bhutan: a review. Crop Protect. 90, 117–124.

Tucci, M., Grattieri, M., Schievano, A., Cristiani, P., Minteer, S.D., 2019. Microbial amperometric biosensor for online herbicide detection: photocurrent inhibition of *Anabaena variabilis*. Electrochim. Cata. 302, 102–108.

Wang, F., Ren, F.C., Li, Y.J., Liu, J.K., 2010. Scutebarbatines W − Z, new *neo*-clerodane diterpenoids from *Scutellaria barbata* and structure revision of a series of 13-spiro *neo*-clerodanes. Chem. Pharm. Bull. 58, 1267–1270.

Wang, T.S., Wang, S.Q., Xiao, D.L., 2012. A review of phytochemistry and antitumor activity of a valuable medicinal species: *Scutellaria barbata*. J. Med. Plants Res. 6, 4259–4275.

Wang, M.L., Chen, Y.Y., Hu, P., Ji, J.Y., Li, X., Chen, J.W., 2018. *neo*-Clerodane diterpenoids from *Scutellaria barbata* with cytotoxic activities. Nat. Prod. Res. https://doi.org/10.1080/14786419.2018.1514399.

Wang, L., Chen, W., Li, M., Zhang, F., Chen, K., Chen, W., 2019. A review of the ethnopharmacology, phytochemistry, pharmacology, and quality control of *Scutellaria barbata* D. Don. J. Ethnopharmacol. https://doi.org/10.1016/j.jep.2019.112260.

Wei, W.J., Song, Q.Y., Zheng, Z.Q., Yao, X.J., Li, Y., Gao, K., 2018. Phytotoxic *ent*-isopimarane-type diterpenoids from *Euphorbia hylonoma*. J. Nat. Prod. 81, 2381–2391.

Wu, T., Wang, Q., Jiang, C., Morris-Natschke, S.L., Cui, H., Wang, Y., Yan, Y., Xu, J., Lee, K.H., Gu, Q., 2015. *neo*-Clerodane diterpenoids from *Scutellaria barbata* with activity against Epstein-Barr virus lytic replication. J. Nat. Prod. 78, 500–509.

Xue, G.M., Xia, Y.Z., Wang, Z.M., Li, L.N., Luo, J.G., Kong, L.Y., 2016. *neo*-Clerodane diterpenoids from *Scutellaria barbata* mediated inhibition of P-glycoprotein in MCF-7/ADR cells. Eur. J. Med. Chem. 121, 238–249.

Yang, G.C., Liang, C., Li, S.G., Liu, M., Jia, M.J., Xu, X.N., Wang, X.B., Hua, H.M., Sun, L.X., 2017. *neo*-Clerodane diterpenoids from aerial parts of *Scutellaria barbata*. Phytochem. Lett. 19, 1–6.

Yeon, E.T., Lee, J.W., Lee, C., Jin, Q., Jang, H., Lee, D., Ahn, J.S., Hong, J.T., Kim, Y., Lee, M.K., Hwang, Y.B., 2015. *neo*-Clerodane diterpenoids from *Scutellaria barbata* and their inhibitory effects on LPS-induced nitric oxide production. J. Nat. Prod. 78, 2292–2296.

Yuan, Q.Q., Song, W.B., Wang, W.Q., Xuan, L.J., 2017. Scubatines A − F, new cytotoxic *neo*-clerodane diterpenoids from *Scutellaria barbata* D. Don. Fitoterapia 119, 40–44.

Yuan, Y., Tian, J.M., Xiao, J., Shao, Q., Gao, J.M., 2014. Bioactive metabolites isolated from *Penicillium sp.* YY-20, the endophytic fungus from *Ginkgo biloba*. Nat. Prod. Res. 28, 278–281.

Zhao, J., Guo, B., Onakpa, M.M., Wong, T., Wakasa, K., Che, C.T., Warpeha, K., 2017. Activity of icacinol from *Icacina trichantha* on seedling growth of *Oryza sativa* and *Arabidopsis thaliana*. J. Nat. Prod. 80, 3314–3318.

Zhu, F., Di, Y.T., Liu, L.L., Zhang, Q., Fang, X., Yang, T.Q., Hao, X.J., He, H.P., 2010. Cytotoxic *neo*-clerodane diterpenoids from *Scutellaria barbata*. J. Nat. Prod. 73, 233–236.

Zhu, F., Di, Y.T., Li, X.Y., Liu, L.L., Zhang, Q., Li, Y., Hao, X.J., He, H.P., 2011. *neo*-Clerodane diterpenoids from *Scutellaria barbata*. Planta Med. 77, 1536–1541.